International Conference on Ships and Offshore Structures
ICSOS 2020
1 – 3 September 2020, Glasgow, UK

Dynamic response of a multi-purpose floating offshore structure under extreme sea conditions

Abhinav K. A[a], Xue Xu [a,*], Zi Lin [a], Maurizio Collu [a]

[a]*Department of Naval Architecture, Ocean and Marine Engineering, University of Strathclyde, Glasgow, UK, G4 0LZ*

Abstract

A novel multi-purpose platform (MPP) has been proposed for providing renewable energy to an offshore fish aquaculture system. After having previously analyzed its dynamic response in operational conditions, it is essential to check its survivability under extreme environmental conditions, focusing on wind speeds and wave heights and periods, for checking serviceability criteria and human factors' requirements. An environmental contour method is applied to derive the 25-year return period extreme metocean conditions, choosing as location the west coast of Scotland (longitude $-7°$, latitude $56.5°$), based on a database of hindcast wind and wave conditions for this location from the start of 2008 till the end of 2017, with a 6 hours granularity. Then, an aero-hydro-servo-elastic coupled model of dynamics of the MPP, in the time domain, is developed, and the dynamic response of the MPP to the 25-year return extreme environment conditions are assessed. The survivability of the MPP under the most extreme environment conditions, have also been checked. The response of the MPP with respect to barge motion and the hub acceleration of wind turbines were observed to fall within the criteria specified in literature.

Keywords: multi-purposa platform; offshore wind turbines; extreme sea conditions; dynamic responses.

1. Introduction

On account of climate change and sustainable development, there has been a continuous upsurge in the progress of renewable energy technologies. Consequently, conventional energies have been progressively substituted by energy from cleaner, renewable sources. Worldwide, the capacity of renewable energy generation has seen an increase of 7.4% since 2019, with wind energy has an expansion of 60 GW out of 176 GW in total (IRENA, 2020). Meanwhile, the increased use of renewables, primarily in the power division, has contributed to a reduction of 215 Mt CO_2 emissions in 2018. More specifically, China and Europe have been the top two in the savings from renewables, accounting for 70% of global total (IEA., 2019). In addition, in Scotland, the strategy is to reach an equivalent 50% of the energy for heat, transport and electricity consumption from renewable sources by 2030 (www.gov.scot., n.d.).

One of the reasons for the growth in the share of renewables is due to their low operating costs and preferential access over other power systems (IEA., 2020). Nonetheless, nowadays one main hindrance in averting the expansion of large-scale ocean renewable energies is the high costs (Astariz *et al.*, 2015). One reason for it is due to the harsher environment conditions in which they operate, subjecting them to a higher degree of risk, compared to onshore structures. Therefore, the O&M cost for large-scale ocean renewable energy devices is much larger than the onshore ones (Astariz *et al.*, 2015). For instance, for offshore wind farms, operation & maintenance (O&M) costs typically account for 25-30% of total lifecycle costs (Rockmann *et al.*, 2017). One acceptable solution for reducing the costs is to have a synergy of various types of energy and food productions, including energy extraction (wind, solar, wave and tidal, etc.), transportation and aquaculture (Rockmann *et al.*, 2017). Following this trend, the selection

* Corresponding author. *E-mail address: xue.xu@strath.ac.uk*

of integrating wind and wave energy devices have become popular since the past decade (Perez-Collazo *et al.*, 2015). For example, a feasibility study of combining a spar-type wind turbine and a wave energy converter (WEC) was studied by Karimirad and Koushan (2016), which claimed that the optimized performance of the wind turbine can be realized by selecting a proper power take-off. Besides, offshore wind turbine support structures cost can be up to 25 % of the capital cost. On this account, Wang, *et al.* carried out a feasibility study on a hybrid offshore wind turbine support structure, derived from the conventional monopile configuration (Wang *et al.*, 2018). Results indicated that the proposed foundation achieves a higher cyclic capability compared with traditional ones. In another example, Cao *et al.* (2017) analyzed a hybrid ocean going platform harvesting wind, solar and wave energies. Results claimed that the utilization of a hybrid energy harvesting system has the advantage of preserving a stable power supply. Due to the complementarity of different energy production between wind and solar throughout the year, the generated energy output has a smaller variation compared with energy from a single source. Furthermore, multiple-use platforms with a synergy of different activities in one platform, have the advantage of saving ocean spaces (Stuiver *et al.*, 2016). This advantage is significant for packed sea zones, where different commercial subdivisions need to be built and managed properly. To this end, the European Union (EU) has announced the policy of handling different economic subdivisions (Gallou, 2018). Therefore, in this paper, we have focused on the design & analysis of a novel MPP for supplying renewable energy to an offshore aquaculture farm.

Compared with extracting ocean energy from a single source, the concept of multi-use platform is an unindustrialized concept (Gallou, 2018). There are no fit-for-purpose design guidelines on it. A commonly accepted method is to follow the traditional design guidelines for offshore structures, for example, DNVGL-RP-C205 (2017) and DNVGL-ST-0119 (2018). These structures are designed to operate and survive in normal and extreme ocean environment. Based on a joint probability model, the design rules & guidelines for traditional offshore structures have been well developed since the past few decades. Nonetheless, today the environmental contour method remains popular as it estimates the long-term extreme responses in a highly efficiency way, relying on a limited number of short-term met ocean conditions only (Ross *et al.*, 2020). Due to the difference between offshore oil & gas platforms and offshore wind turbines, traditional design methods may no longer be suitable for offshore renewable energy devices. For this reason, Li *et al.* (2016) re-developed the conventional environmental contour method for the analysis of offshore bottom fixed wind turbines. It is claimed that in terms of long-term extreme, the modified method can detect the overriding environmental condition. Velarde *et al. (2019)* applied the environmental contour method to investigate the extreme resonant response of offshore wind turbines. Case studies on an offshore monopile wind turbine showed that the resonant loads play a leading role. Existing studies have focused on the analysis of marine renewable energy devices with a single energy extraction source (Manuel *et al.*, 2018) or a combined wind and wave energy convertor (Li *et al.*, 2018). Fewer studies have focused on the analysis of an offshore multi-use platform under extreme condition based on the environmental contour approach. This paper applied the environmental contour method to analyze the response of a novel MPP for supplying power and fish feed to an offshore aquaculture farm. The detailed environmental contour methodology is described in Section 2 and its application on the MPP is explained in Section 3. The paper concludes with Section 4.

Nomenclature

$f_{(u)}$	distribution function
h_0	shifting point of *Hs*
Hs	significant wave height
P(u)	cumulative distribution of the wind speed
Tp	peak wave period
u	wind speed
V_{10}	mean wind speed at 10m above SWL
α	shape parameter for Weibull distribution
β	scale parameter for Weibull distribution
σ_{LTC}	standard deviation
μ_{LTC}	mean value

Subscript

HC parameter for significant wave hight
u parameter for wind speed

2. The 25-year return environmental contour

For the metocean data measured at the offshore coast of Scotland (longitude -7°, latitude 56.5°), the mean wind speed data were measured at 10m above SWL. To find out the joint distribution of mean wind speed (V_{10}), significant wave height (*Hs*) and peak wave period (*Tp*), the single distribution of V_{10} will need to be calculated first. Then, the conditional distribution of *Hs* on given V_{10} and the conditional distribution of *Tp* on given *Hs* will be calculated. Finally, the 3-D environmental contour can be created by using the Rosenblatt transformation. The wave scatter diagram at the site under consideration, is shown in Fig. 1.

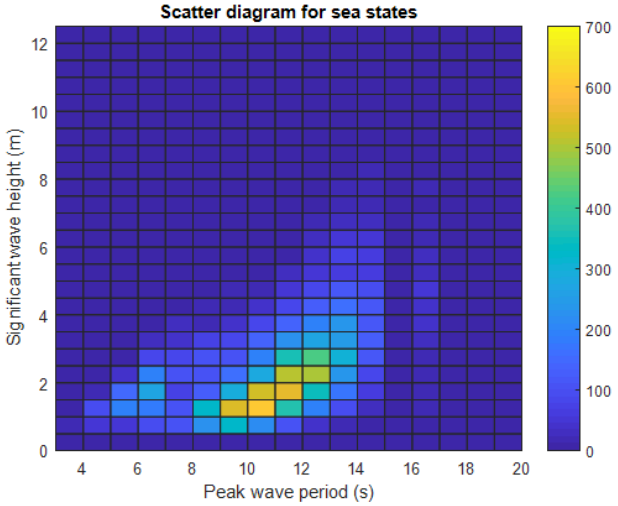

Fig. 1 Wave scatter diagram at the offshore coast of Scotland (longitude -7°, latitude 56.5°)

2.1. Cumulative distribution of V_{10}

Weibull distribution is proved to be a good model for the wind speed distribution (Li *et al.*, 2015), the equation is shown below:

$$f_{U_w(u)} = \frac{\alpha_U}{\beta_U}\left(\frac{u}{\beta_U}\right)^{\alpha_U - 1} \cdot \exp\left[-\left(\frac{u}{\beta_U}\right)^{\alpha_U}\right] \tag{1}$$

where α_U is the shape parameter and β_U is the scale parameter. u represent the wind speed – V_{10}. The 10 years raw wind data Weibull plot is shown in Fig. 2, where $\alpha_{U1} = 2.174$ and $\beta_{U1} = 9.3109$. It is seen that the two parameter Weibull distribution (in the red line) can fit most part with the raw wind data (blue cross). Fig. 3 shows the zoomed in tail part of Fig. 2, where it shows clearly that the Weibull distribution cannot fit with the wind speed above 22 m/s. Thus, to predict the extreme wind speed in a 25-year return (or 50-year and 100-year return), the tail part of the raw data, when the wind speed larger than 22 m/s, another set of Weibull distribution parameters is needed, in order to ensure a better prediction of the extreme wind speeds, as shown in Fig. 4, where a trend line has been created to fit the data and its equation is shown in the figure.

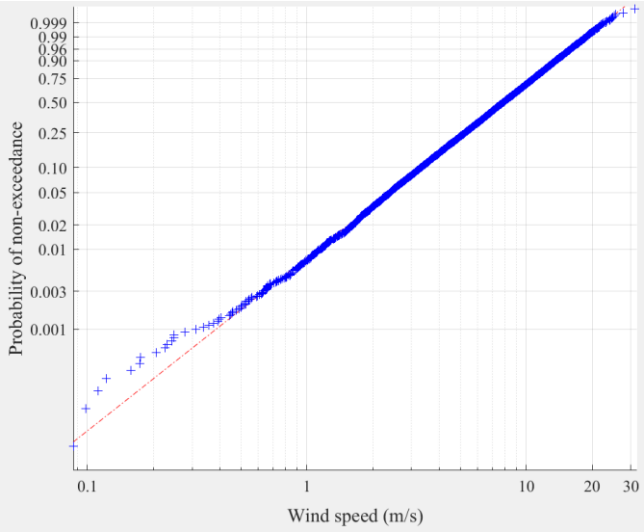

Fig. 2 Weibull plot of V_{10} at Scottish site

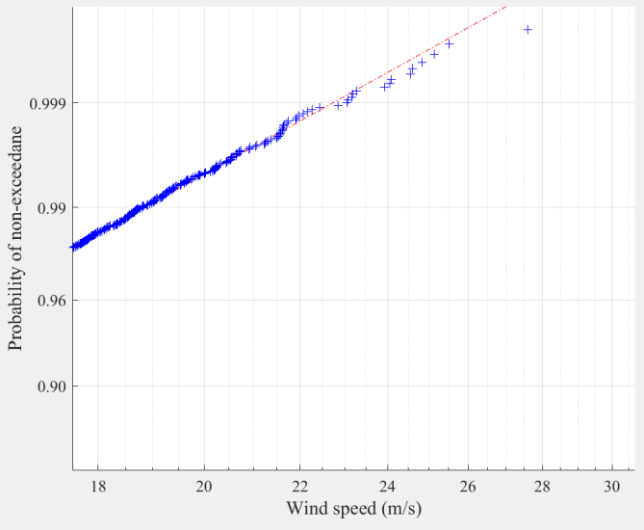

Fig. 3 Zoomed-in tail part of Fig. 2

In Fig. 4, *u* represents the wind speed; *P(u)* is the cumulative distribution of the wind speed, where

$$P(u) = 1 - \exp[-\left(\frac{u}{\beta}\right)^{\alpha}] \quad (2)$$

For $y = mx + c$ in Fig. 4, the $m = \alpha_U$ and $c = -\alpha_U * ln(\beta_U)$. Thus, when wind speed is larger than 22 m/s, $\alpha_{U2} = 1.3867$ and $\beta_{U2} = 5.609$, for the Weibull distribution, it gives a maximum V_{10} = 32.02 m/s for a 25-year return. The maximum wind speed been observed in the 10-year data is 31.25 m/s.

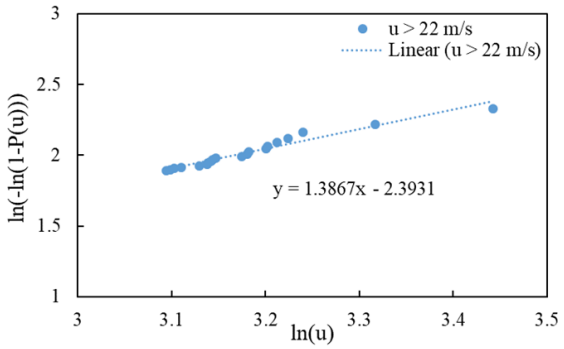

Fig. 4 Fit raw wind data larger than 22 m/s

2.2. Single distribution of Hs

As discussed by Li *et al.* (2015), for single distribution of *Hs*, the lower significant wave height does not follow the Weibull model but the higher ones are suitable. Therefore, for lower wave height, where $Hs < h_0$ (h_0 = 3.2 m in this study), a lognormal distribution can be applied and the equation is shown below. The h represents the *Hs*. Fig. 5 shows the Weibull plot for the all raw data of *Hs* at the Scotland site. It is seen that the higher *Hs* (tail part of Fig. 5) are slightly overestimated by the Weibull distribution, but this will not affect the result of the environmental contour, which using the conditional distribution of *Hs* on given V_{10}. As for the 25-year return, it is the extreme condition been considered, so the Weibull distribution will be used to predict the extreme significant wave height, details are shown in Section 2.3.

$$f_{Hs}(h) = \begin{cases} \dfrac{1}{\sqrt{2\pi}\sigma_{LHM}h} \cdot exp\left[-\dfrac{1}{2}\left(\dfrac{\ln(h)-\mu_{LHM}}{\sigma_{LHM}}\right)^2\right], & h \le h_0 \\ \dfrac{\alpha_{HM}}{\beta_{HM}}\left(\dfrac{h}{\beta_{HM}}\right)^{\alpha_{HM}-1} \cdot exp\left[\left(-\dfrac{h}{\beta_{HM}}\right)^{\alpha_{HM}}\right], & h > h_0 \end{cases} \quad (3)$$

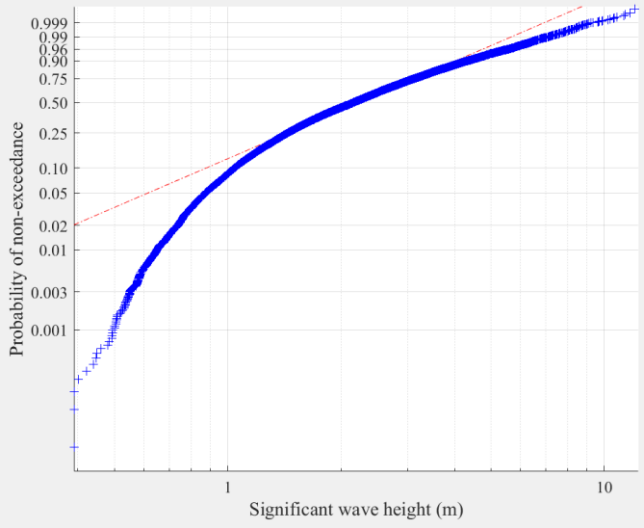

Fig. 5 Weibull plot of Hs at Scottish site

For the Weibull fit part, the $\alpha_{HM} = 1.302$ and $\beta_{HM} = 2.028$, which are calculated at the shifting point (h_0), by using the continuity condition of PDF and cumulative density function. Thus, the single distribution of *Hs*, for 3 hours in 25-year return, its extreme value will be 12.96 m. The maximum *Hs* been observed in the 10 years' data is 12.04 m.

2.3. Conditional distribution of Hs on given V_{10}

The cumulative conditional distribution of *Hs* on given V_{10} follows the two-parameter Weibull distribution, and the equation is shown below:

$$P(h) = 1 - \exp\left[-\left(\frac{h}{\beta_{HC}}\right)^{\alpha_{HC}}\right] \tag{4}$$

$$\alpha_{HC} = a_1 + a_2 \cdot u^{a_3} \tag{5}$$

$$\beta_{HC} = b_1 + b_2 \cdot u^{b_3} \tag{6}$$

where the α_{HC} is the shape parameter and β_{HC} is the scale parameter. The parameters from a_1 to b_3 are calculated by the curve fitting with the raw data (bin size of the wind data is 1 m/s, i.e. for each group of Hs, it will give a set of α_{HC} and β_{HC}). Fig. 6 shows the fit curves for α_{HC} and β_{HC} according to the whole group of raw data. Again, when the wind speed is larger than about 20 m/s, the tail curve cannot fit very well.

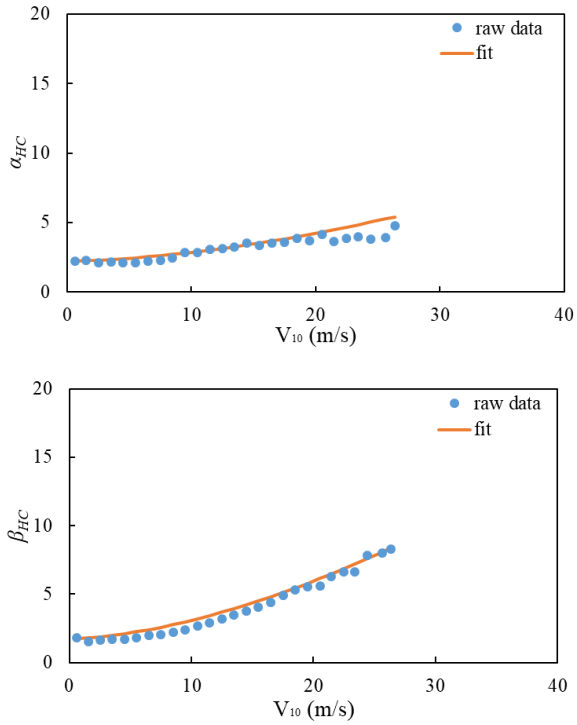

Fig. 6 Whole group of raw data fitting of α_{HC} and β_{HC} for conditional distribution of *Hs* on given V_{10} at the Scottish site

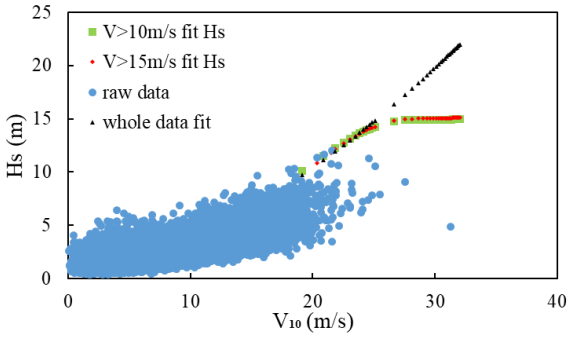

Fig. 7 Conditional distribution of *Hs* on given V_{10} with different groups of wind speed on a series return period

As shown in Fig. 7, the line with 'black triangle' dots represent the predicted *Hs* on given wind speed, which shape and scale parameters are calculated by fitting all wind bin groups, and are predicted with the return period from 1 months, 2 months,…, 12 months (1 year), 2 years,…, to 25 years, where the

$$\alpha_{HC} = 2.148 + 0.2818u^{0.7119} \tag{7}$$

$$\beta_{HC} = 1.402 + 0.0316u^{1.731} \tag{8}$$

However, as shown in Fig. 7, the calculated parameters cannot predict the tail part of the *Hs* very well, which givens *Hs* in 25-year return is 22.00 m when V_{10} is 32.02 m/s, which is too large for real scenarios. Thus, considering that it is the extreme conditions are inrested in this study, the parameters will be fitted with wind speeds are larger than 10 m/s, 15m/s and 20 m/s, respectively, and then choose the most suitable curves to predict the *Hs* on given V_{10}. In addition, when wind speed is between 23 m/s to 24 m/s, the shape parameter is too far away from the curve trend, as shown in Fig. 6, so this set of data has been excluded when curve fitting.

When fit the *Hs* where V_{10} > 10 m/s, the *Hs* in 25-year return is 14.98 m on given V_{10} = 32.02 m/s, which gives

$$\alpha_{HC1} = 4.115 + 1.348 \times 10^{-15}u^{10.6} \tag{9}$$

$$\beta_{HC1} = 0.06266 + 0.1485u^{1.287} \tag{10}$$

In addition, when the wind speed is between 29.02 m/s to 30.50 m/s, there is a small decrease of *Hs* from 14.93 m to 14.91 m, and then the *Hs* start to increase slowly with the increase of the wind speeds.

When fit the *Hs* where V_{10} > 15 m/s, the *Hs* in 25-year return is 15.15 m on given V_{10} = 32.02 m/s, which gives

$$\alpha_{HC2} = 4.138 + 1.156 \times 10^{-15}u^{10.64} \tag{11}$$

$$\beta_{HC2} = 0.8414 + 0.08525u^{1.432} \tag{12}$$

There shows no drop down of Hs in this group of fit parameters calculation.

When fit the *Hs* where V_{10} > 20 m/s, the *Hs* in 25-year return is 40.35 m on given V_{10} = 32.02 m/s, which is to far beyond the real scenario. Thus, this group of data will not be considered.

Consequently, considering the amount of data been analyzed, the tiny differences between the parameters fit with data group when V_{10} > 10 m/s and V_{10} > 15 m/s, and the similar decrease trend with the raw data at the extreme conditions, α_{HC1} and β_{HC1} will be used to calculated the *Hs* on given V_{10}. For α_{HC1}, the term $1.348 \times 10^{-15}u^{10.6}$ seems can only give very small values and α_{HC1} can be treated as a constant – 4.115. But this proves to be not true, as when considering the maximum wind speed in 25-year return, which is 32.02 m/s, it gives

$$1.348 \times 10^{-15}u^{10.6} = 12.2353 \tag{13}$$

which is almost three times larger than 4.115. In addition, if $\alpha_{HC1} = 4.115$ been applied, the maximum *Hs* on given wind speed in 25-year return will be 23.24 m, which also is too high for realistic wave height.

2.4. Conditional distribution of Tp on given Hs

According to the Li *et al.* (2015), the conditional distribution of *Tp* on given *Hs* follows a lognormal distribution, as shown in the equation below where the μ_{LTC} is the mean value and σ_{LTC} is the standard deviation of *ln (t)*. *t* represents the *Tp*; *h* represents *Hs*.

$$f_{T_p|H_s}(t|h) = \frac{1}{\sqrt{2\pi}\sigma_{LTC}t} \cdot \exp\left[-\frac{1}{2}\left(\frac{\ln(t) - \mu_{LTC}}{\sigma_{LTC}}\right)^2\right] \tag{14}$$

$$\mu_{LTC} = c_1 + c_2 \cdot h^{c_3} \tag{15}$$

$$\sigma_{LTC}^2 = d_1 + d_2 \cdot \exp(d_3 h) \tag{16}$$

Similar with the results shown in Fig. 6, the parameters from c_1 to d_3 are calculated by the curve fitting with the raw data. The *Tp* is estimated with a bin size of 0.5 m for different *Hs*. In this study,

$$\mu_{LTC} = 0.8916 + 1.272h^{0.1753} \tag{17}$$

$$\sigma^2_{LTC} = 0.00001 + 0.1476e^{-0.4073h} \tag{18}$$

which gives the *Tp* for a 25-year return, 3 hours, on given *Hs* = 14.98 m, is 17.25 s.

2.5. the 25-year return environmental contour

By applying the Rosenblatt transformation with the joint distributions obtained above, a contour surface can be obtained for the 25-year return predictions. Fig. 8 shows the 25-year return environmental data at different projection areas, where each wind speed links with a specifit significant wave height and peak wave period. The colour bar shows the wind speeds with differenct colour. Fig. 9 presents some example environmental contour lines of the *Hs* and *Tp* at different wind speeds. It is seen that with the increasing of the wind speeds, the significant wave height values are increasing and the peak wave period are getting higher. The most extreme environmental conditions is shown in Fig. 9 (g), where V_{10} = 32.0232 m/s, *Hs* = 14.98 m and *Tp* = 17.25 s. The selecte load cases (as shown in Table 1) will be applied to the MPP for numerical simulations.

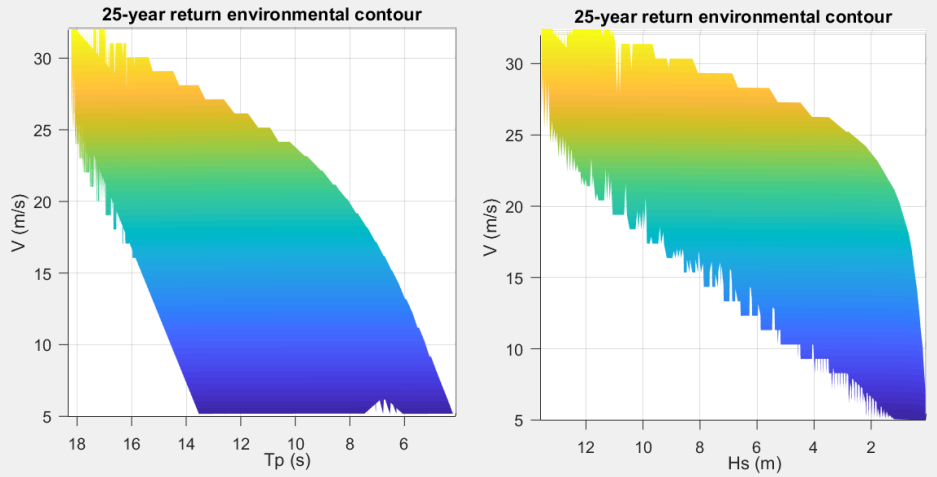

(a) y and z-axis projection area (b) x and z-axis projection area

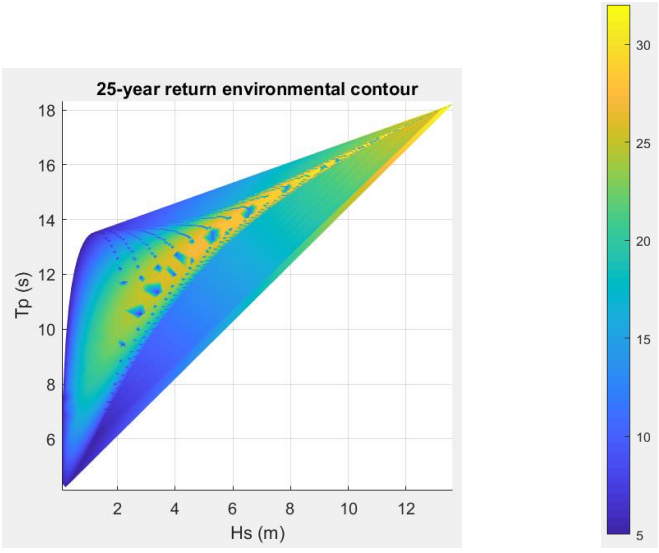

(c) x and y-axis projection area

Fig. 8 Projection area of the 25-year return environmental contour

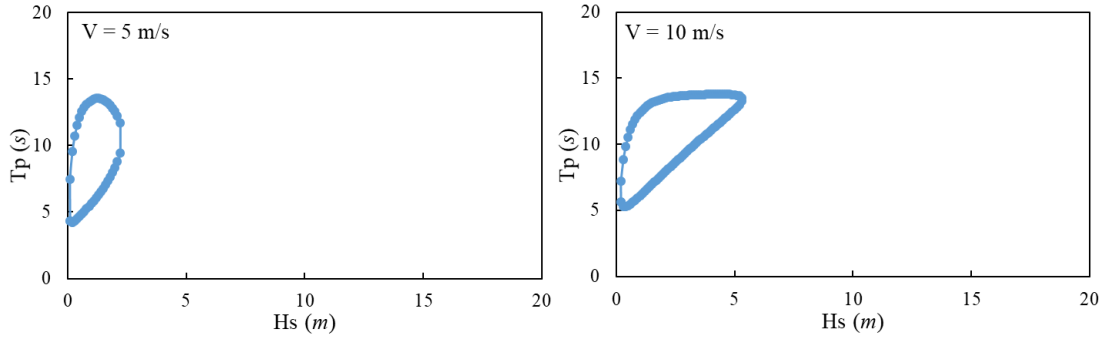

(a) V_{10} = 5m/s

(b) V_{10} = 10m/s

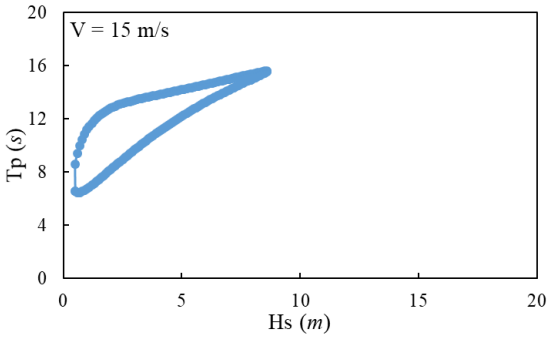

(c) V_{10} = 15m/s

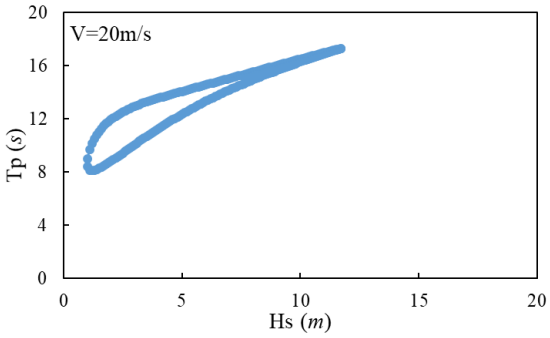

(d) V_{10} = 20m/s

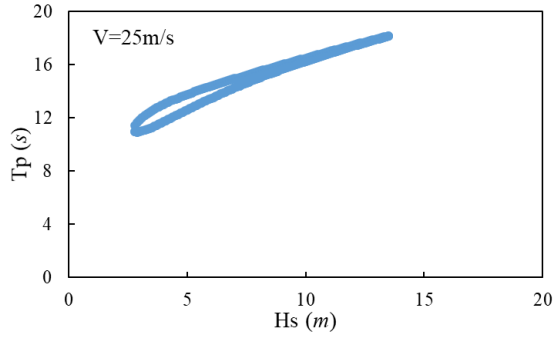

(e) V_{10} = 25m/s

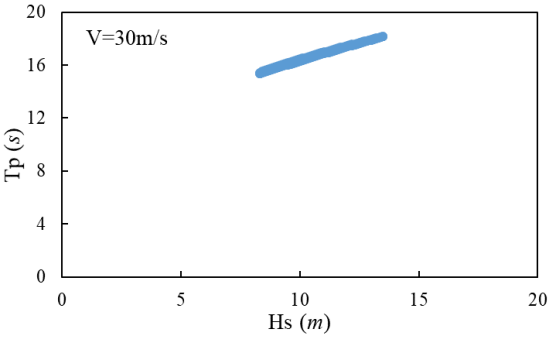

(f) V_{10} = 30m/s

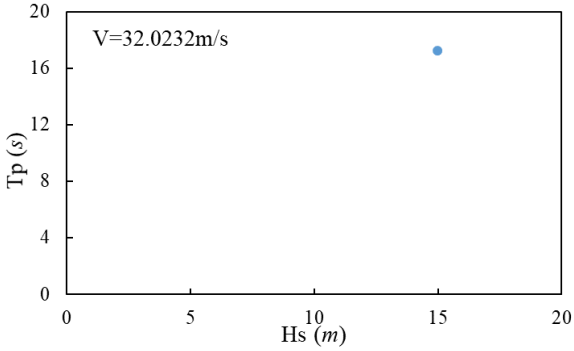

(g) V_{10} = 32.0232m/s

Fig. 9 Tp and Hs at different wind speeds, 25-year return

3. Dynamic response of the MPP

The environmental contour methodology described in Section 2 is now used to analyze the dynamic response of an MPP to combined wind and wave loading. The MPP is obtained by retrofitting a feed barge with 4 small rated wind turbines. For further info please refer to (Abhinav *et al.*, 2019). This MPP serves the dual purpose of supplying fish feed and renewable energy to an offshore aquaculture farm. The main features of the energy feed barge and the wind turbines are stated in the Table 2 and Table 3, respectively. A plan view of the MPP is shown in Fig. 10.

Table 2 Feed barge properties.

Description	Value
Feed storage capacity	600 tons
Length	37.2 m
Beam	12 m
Hull depth	5.2 m
Minimum freeboard	1.332 m

Table 3 Wind Turbines.

Parameter	Aeolos - H 20	Polaris P10-20
Cut-in wind speed (m/s)	3.0	2.7
Rated wind speed (m/s)	10	11
Cut-out wind speed (m/s)	25	25
Rated power (kW)	20	20
Rotor diameter (m)	10	10
Rotor speed (RPM)	90	100

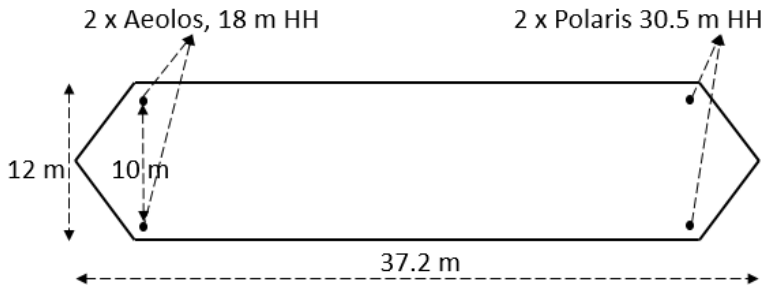

Fig. 10 Plan view of the MPP (Abhinav *et al.*, 2019)

The coupled aerodynamic-hydrodynamic time domain analyses are performed using the commercial software SIMA (DNVGL-ST-0119, 2018). Due to limitations in SIMA, the four wind turbines in the MPP are replaced with an single one at the center, such that the sum of the maximum thrust force and overturning moments produced by the four wind turbines are equal to that generated by the equivalent turbine (Abhinav *et al.*, 2019). The mooring systems comprise of 8 catenary lines comprised of chain and polyester rope, with a pre-tension of 1 MN.

TurbSim (Jonkman, 2009) is used as a pre-processor for building stochastic wind fields which are used as input for SIMA. The wind speed time series generated at discrete points along a 2-dimensional grid encompassing the rotor are now added to the model in SIMA. The generation of irregular waves are realized from the JONSWAP spectrum. Wind loads on the turbine blades and wave loads on the mooring lines are simulated using an expanded version of the blade element momentum theory (Hansen, 2000) and the Morison equation (Morison *et al.*, 1950), respectively. Time domain response is calculated using the convolution integral method. The numerical model of the MPP generated in SIMA is shown in Fig. 11.

The time domain equation of motion can be written as follows, for a moored or freely floating body:

$$[m + A(\omega)]\ddot{x} + C(\omega)\dot{x} + Kx = f'(t) = q - D_2 f(\dot{x}) - D_2\dot{x} \tag{19}$$

Here m is the body mass matrix, A is the frequency dependent added mass matrix, C is the frequency dependent potential damping matrix, K is the hydrostatic stiffness matrix, x is the position vector, f is a vector function, q is the exciting force vector and D_1, D_2 are the linear and quadratic damping matrices, respectively. Applying the following:

$$A(\omega) = A_\infty + a(\omega), A_\infty = A(\omega = \infty) \tag{20}$$

$$C(\omega) = C_\infty + c(\omega), C_\infty = C(\omega = \infty) \tag{21}$$

Applying the inverse Fourier transform, considering that the values of $h(t-\tau)$ is 0, for $(t<0)$:

$$A_\infty\ddot{x}(t) + a(\omega), A_\infty = A(\omega = \infty) \tag{22}$$

the equation of motion now becomes:

$$[m + A_\infty]\ddot{x} + D_1\dot{x} + D_2 f(\dot{x}) + Kx + \int_0^t h(t-\tau)\dot{x}(\tau)d\tau = q(t, x, \dot{x}) \tag{23}$$

The frequency dependent added-mass and damping can be transformed to obtain the retardation function $h(\tau)$:

$$h(\tau) = \frac{1}{2\pi}\int_{-\infty}^{\infty}[c(\omega) + i\omega a(\omega)]e^{i\omega t}d\omega = \frac{1}{2\pi}\int_{-\infty}^{\infty}H(\omega)e^{i\omega t}d\omega \tag{24}$$

The transfer function of the response is:

$$H(\omega) = \int_{-\infty}^{\infty}h(\tau)e^{i\omega t}d\tau = c(\omega) + i\omega a(\omega) \tag{25}$$

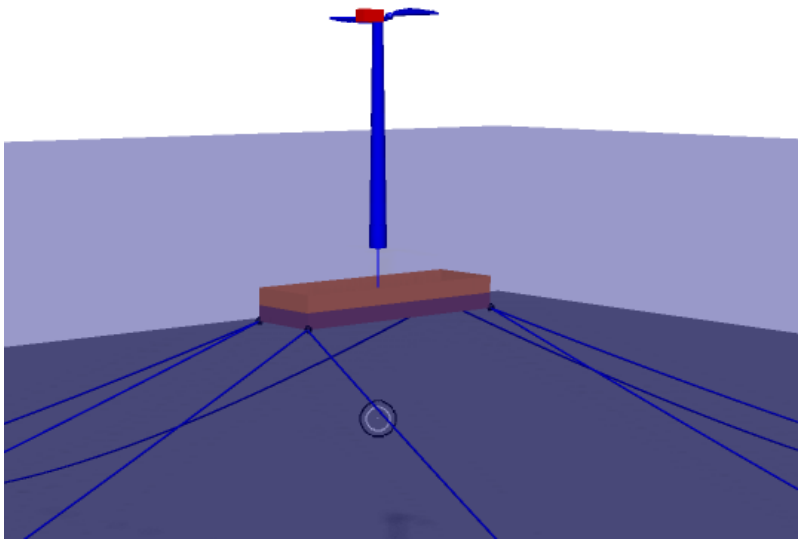

Fig. 11 SIMA model of MPP

Each simulation is run for 4200 s and the first 600 s are ignored to account for the start-up transients. Thus, each output time series has a length of 3600 s or 1 hour. 10 separate analyses are conducted for each met-ocean condition (i.e. sea-state and associated wind speed), using different wind and wave time series and the ensemble averages are reported. This would help in eliminating the epistemic uncertainty arising from the use of a single time history (Dong *et al.*, 2012).

The met-ocean conditions correspond to a return period of 25 years, as derived using the environmental contours and are listed in Table 4. Three different hub height wind speeds are considered

– 5 m/s, 10 m/s and 20 m/s. For the first two, sea-states corresponding to the maximum wave height are chosen. However, for the wind speed of 20 m/s, a lower wave height is considered, as the MPP is dimensioned to withstand a significant wave height lesser than 6 m, only.

Table 4 Met-ocean conditions.

Sl. No.	V (m/s)	Hs (m)	Tp (s)
1	5	2.2	11.72
2	10	5.3	13.53
3	20	5.4	14.26

The dynamic response of the MPP is compared against the NORDFORSK (1987) criteria that lays out the maximum limits on motions and accelerations, with respect to a safe and healthy operational environment within the barge. The work done onboard barges is classified as heavy manual work (Mathisen, 2012), with corresponding limiting values of roll, vertical and lateral accelerations being defined as 4.0°, 0.15 g and 0.07 g, where g is the gravitational acceleration constant. Table 5 shows the ensemble averaged RMS values of the cabin level accelerations and roll, for the different met-ocean conditions (defined as MC, with reference to Table 3), which are observed to be lower in comparison with the NORDFORSK criteria.

Table 5 RMS values - Roll and acceleration for barge.

MC No.	Roll (°)	Vertical acceleration	Lateral acceleration
1	0.02	0.018 g	0.031 g
2	0.10	0.038 g	0.068 g
3	0.17	0.037 g	0.067 g

A further consideration is investigated with respect to the dynamic response of the wind turbines onboard the barge. The limiting hub accelerations for wind turbines has been defined in literature as 0.5 g to 0.6 g (Collu and Borg, 2016). The maximum lateral (fore-aft) hub-height accelerations are shown in Table 6. The accelerations are obtained as averages of the two wind turbines at the same hub-height. The hub-height acceleration criteria for wind turbines can be observed to be satisfied for all the three met-ocean conditions.

Table 6 Hub height (HH) acceleration for wind turbines

MC No.	HH - 18 m	HH – 30.5 m
1	0.05 g	0.07 g
2	0.10 g	0.14 g
3	0.09 g	0.13 g

4. Conclusions

The dynamic response to wind and wave conditions of a novel MPP in the shape of a feeding barge retrofitted with 4 small wind turbines, with the function of supplying feed and power to an offshore aquaculture farm, has been investigated.

The 25-year return environmental contour has been derived by using the Rosenblatt transoformation, combining the single wind speed distribution, conditional distribution of significant wave height on given wind speed, and conditional distribution of peak wave period on given significant wave height. Three of the met-ocean conditions have been selected to investigate the MPP responses.

For the met-ocean conditions investigated, the response of the MPP was found to satisfy the requirements found in literature, with respect to barge motion and hub-acceleration of the wind turbines. The safe operational characteristics of the MPP concept indicates its suitability for use in offshore aquaculture farms, eliminating the need for diesel generators.

Acknowledgements

The authors would like to thank the UK-China Centre for Offshore Renewable Energy (CORE) for funding the present work, through the Flexible Funding program. The authors also acknowledge the help rendered by Hongyang Dong, Research Fellow, University of Warwick, in preparing the funding proposal. The authors are also thankful to the EPSRC projects INNO-MPP (EP/R007497/2) and FENGBO-WIND (EP/R007470/1) for supporting the work.

References

Abhinav, K., Collu, M., Ke, S. & Binzhen, Z. Frequency Domain Analysis of a Hybrid Aquaculture-Wind Turbine Offshore Floating System. ASME 2019 38th International Conference on Ocean, Offshore and Arctic Engineering, 2019. American Society of Mechanical Engineers Digital Collection.

Astariz, S., Perez-Collazo, C., Abanades, J. & Iglesias, G. 2015. Co-located wave-wind farms: Economic assessment as a function of layout. *Renewable Energy,* 83**,** 837-849.

Cao, Y., Townsend, N. & Tan, M. Hybrid renewable energy system for ocean going platforms. OCEANS 2017-Aberdeen, 2017. IEEE, 1-7.

Collu, M. & Borg, M. 2016. Design of floating offshore wind turbines. *Offshore Wind Farms.* Elsevier.

DNVGL-RP-C205 2017. Environmental conditions and environmental loads. *Det Norske Veritas group, Norway*.

DNVGL-ST-0119 2018. Floating wind turbine structures. *Det Norske Veritas group, Norway*.

Dong, W., Xing, Y. & Moan, T. 2012. Time domain modeling and analysis of dynamic gear contact force in a wind turbine gearbox with respect to fatigue assessment. *Energies,* 5**,** 4350-4371.

Gallou, M. L. 2018. *Multi-use ocean platforms: an emerging concept.* [Online]. Maritime Forum - European Commission. Available: Maritime Forum - European Commission. [Accessed 19 May 2020].

Hansen, M. O. 2000. *Aerodynamics of wind turbines: rotors, loads and structure*, Earthscan.

IEA. 2019. *Emissions – Global Energy & CO2 Status Report 2019 – Analysis.* [Online]. Available: https://www.iea.org/reports/global-energy-co2-status-report-2019/emissions#abstract. [Accessed].

IEA. 2020. *Global energy and CO2 emissions in 2020 – Global Energy Review 2020 – Analysis.* [Online]. Available: https://www.iea.org/reports/global-energy-review-2020/global-energy-and-co2-emissions-in-2020#abstract. [Accessed].

IRENA 2020. Renewable capacity highlights.

Jonkman, B. J. 2009. TurbSim user's guide: Version 1.50. National Renewable Energy Lab.(NREL), Golden, CO (United States).

Karimirad, M. & Koushan, K. 2016 WindWEC: Combining wind and wave energy inspired by hywind and wavestar. IEEE International Conference on Renewable Energy Research and Applications (ICRERA), 2016. IEEE, 96-101.

Li, L., Gao, Z. & Moan, T. 2015. Joint distribution of environmental condition at five european offshore sites for design of combined wind and wave energy devices. *Journal of Offshore Mechanics and Arctic Engineering,* 137.

Li, Q., Gao, Z. & Moan, T. 2016. Modified environmental contour method for predicting long-term extreme responses of bottom-fixed offshore wind turbines. *Marine Structures,* 48**,** 15-32.

Li, Q., Michailides, C., Gao, Z. & Moan, T. 2018. A comparative study of different methods for predicting the long-term extreme structural responses of the combined wind and wave energy concept

semisubmersible wind energy and flap-type wave energy converter. *Proceedings of the Institution of Mechanical Engineers, Part M: Journal of Engineering for the Maritime Environment,* 232**,** 85-96.

Manuel, L., Nguyen, P. T., Canning, J., Coe, R. G., Eckert-Gallup, A. C. & Martin, N. 2018. Alternative approaches to develop environmental contours from metocean data. *Journal of Ocean Engineering and Marine Energy,* 4**,** 293-310.

Mathisen, S. 2012. *Design criteria for offshore feed barges.* Institutt for marin teknikk.

Morison, J., Johnson, J. & Schaaf, S. 1950. The force exerted by surface waves on piles. *Journal of Petroleum Technology,* 2**,** 149-154.

Nordforsk 1987. The Nordic Cooperative Project, Seakeeping Performance of Ships Assessment of a Ship's Performance in a Seaway. *Marintek, Trondheim*.

Perez-Collazo, C., Greaves, D. & Iglesias, G. 2015. A review of combined wave and offshore wind energy. *Renewable and Sustainable Energy Reviews,* 42**,** 141-153.

Rockmann, C., Lagerveld, S. & Stavenuiter, J. 2017. Operation and maintenance costs of offshore wind farms and potential multi-use platforms in the Dutch North Sea. *Aquaculture Perspective of Multi-Use Sites in the Open Ocean.* Springer, Cham.

Ross, E., Astrup, O. C., Bitner-Gregersen, E., Bunn, N., Feld, G., Gouldby, B., Huseby, A., Liu, Y., Randell, D. & Vanem, E. 2020. On environmental contours for marine and coastal design. *Ocean Engineering,* 195**,** 106194.

Stuiver, M., Soma, K., Koundouri, P., Van Den Burg, S., Gerritsen, A., Harkamp, T., Dalsgaard, N., Zagonari, F., Guanche, R. & Schouten, J.-J. 2016. The Governance of multi-use platforms at sea for energy production and aquaculture: challenges for policy makers in European seas. *Sustainability,* 8**,** 333.

Velarde, J., Vanem, E., Kramhøft, C. & Sørensen, J. D. 2019. Probabilistic analysis of offshore wind turbines under extreme resonant response: Application of environmental contour method. *Applied Ocean Research,* 93**,** 101947.

Wang, X., Zeng, X., Yang, X. & Li, J. 2018. Feasibility study of offshore wind turbines with hybrid monopile foundation based on centrifuge modeling. *Applied Energy,* 209**,** 127-139.

www.gov.scot. n.d. *The future of energy in Scotland: Scottish energy strategy - gov.scot.* [Online]. Available: https://www.gov.scot/publications/scottish-energy-strategy-future-energy-scotland-9781788515276/ [Accessed 19 May 2020].